Creating a virtual source inside a medium from reflection data: a stationary-phase analysis

Kees Wapenaar[1], Filippo Broggini[2] & Roel Snieder[2]

[1] *Department of Geotechnology, Delft University of Technology, P.O. Box 5048, 2600 GA Delft, The Netherlands*
[2] *Center for Wave Phenomena, Colorado School of Mines, Golden, CO 80401, USA*

ABSTRACT

With seismic interferometry a virtual source can be created inside a medium, assuming a receiver is present at the position of the virtual source. Here we discuss a method that creates a virtual source inside a medium from reflection data, without needing a receiver inside the medium. Apart from the reflection data, an estimate of the direct arrivals is required. However, no information about the scatterers in the medium is needed. We analyze the proposed method for a simple configuration with stationary-phase arguments. We show that the retrieved virtual-source response correctly contains the multiple scattering coda of the inhomogeneous medium. The proposed method can serve as a basis for data-driven suppression of internal multiples in seismic imaging.

Key words: controlled source seismology, wave scattering and diffraction, interferometry, theoretical seismology.

1 INTRODUCTION

We discuss a new approach to creating the response to a virtual source inside a medium that goes beyond seismic interferometry. Broggini et al. (2011, 2012) propose the 1D version of this new approach. They show that, given the reflection response of a 1D layered medium, it is possible to obtain the response to a virtual source inside the medium, without the need to know the medium parameters. The method consists of an iterative scheme, akin to earlier work of Rose (2001). Interestingly, the response retrieved by this new method contains all scattering effects of the layered medium. Note that in order to obtain the same virtual-source response by seismic interferometry one would need a receiver at the position of the virtual source inside the medium, and real sources at the top and bottom of the medium. Hence, the advantage of the new approach over 1D seismic interferometry is that no receivers are needed inside the medium and that the medium needs to be illuminated from one side only. Broggini & Snieder (2012) speculate that the 1D method can be extended to three dimensions. This would imply that the 3D response to a virtual source in the subsurface could be retrieved from 3D reflection measurements at the surface, without knowing the parameters of the 3D medium. Hence, unlike for controlled-source interferometric methods (Schuster et al., 2004; Bakulin & Calvert, 2006), no receivers would be required in the subsurface, nor would the lack of sources illuminating the medium from below cause spurious multiples (Snieder et al., 2006).

Last year we made a first step towards generalizing the method of Broggini et al. (2011, 2012) to the 3D situation (Wapenaar et al., 2011). Using physical arguments we proposed an iterative scheme that indeed seems to transform the reflection response of a 3D medium into the response to a virtual source inside the medium. The proposed scheme requires, apart from the reflection data, an estimate of the direct arrivals between the virtual source and the acquisition surface. It is, in fact, through this traveltime curve that one specifies the location of the virtual source. Hence, the method is not fully model-independent. Note, however, that a model that relates direct arrivals to a source position can be much simpler than a model that explains all internal multiple scattering. In the proposed method the multiple-scattering part of the virtual-source response comes entirely from the reflection data.

The proposed method has not yet been proven mathematically (except for the 1D situation), nor have the limitations been exhaustively investigated. Here we

analyze the scheme for a simple 2D configuration with the method of stationary phase. We discuss the iterative procedure step-by-step and, en passant, repeat our physical arguments why the method is expected to converge to the virtual-source response, also in more complex situations.

2 THE CONFIGURATION

We consider a configuration of two parallel dipping reflectors in a lossless, constant velocity, variable density medium (Figure 1). The only reason for choosing a constant velocity is that all responses obey simple analytical expressions. However, the proposed scheme is not restricted to constant velocity media. We denote spatial coordinates as $\mathbf{x} = (x, z)$. The acquisition surface is located at $z = 0$ and is transparent (i.e., the upper half-space has the same medium parameters as the first layer). The first dipping reflector obeys the relation $z = z_1 - ax$, with $z_1 = 1000$ m and $a = 1/4$. The red dot denotes the position of the virtual source, with coordinates $\mathbf{x}_{VS} = (x_{VS}, z_{VS}) = (100, 1400)$. The second reflector is chosen parallel to the first reflector, so that all mirror images of the source lie on a line perpendicular to the reflectors. This line obeys the relation $z = z_1 + x/a$. The second reflector crosses this line at $\mathbf{x} = (150, 1600)$. The velocity in the medium is set to $c = 2000$ m/s. The density in the three layers are $\rho_1 = \rho_3 = 1000$ kg/m^3, and $\rho_2 = 5000$ kg/m^3. The reflection coefficients for downgoing waves at the two interfaces are $r_1 = (\rho_2 - \rho_1)/(\rho_2 + \rho_1) = 2/3$ and $r_2 = (\rho_3 - \rho_2)/(\rho_3 + \rho_2) = -2/3$, respectively. The reflection coefficients for upgoing waves are $-r_1$ and $-r_2$. The transmission coefficients for downgoing $(+)$ and upgoing $(-)$ waves are $t_1^{\pm} = 1 \pm r_1$ and $t_2^{\pm} = 1 \pm r_2$.

3 THE REFLECTION RESPONSE AND THE PRIMARY ARRIVALS

We introduce the Green's function $G(\mathbf{x}, \mathbf{x}_S, t)$ as a solution of the wave equation $LG = -\rho\delta(\mathbf{x} - \mathbf{x}_S)\frac{\partial\delta(t)}{\partial t}$, with $L = \rho\nabla\cdot(\rho^{-1}\nabla) - c^{-2}\frac{\partial^2}{\partial t^2}$. Defined in this way, the Green's function is the response to an impulsive point source of volume injection rate at $\mathbf{x}_S$ (de Hoop, 1995). Similar as in seismic interferometry, the Green's function is defined in the true medium. In the frequency domain, $\hat{G}(\mathbf{x}, \mathbf{x}_S, \omega)$ obeys the equation $\hat{L}\hat{G} = -j\omega\rho\delta(\mathbf{x} - \mathbf{x}_S)$, with $\hat{L} = \rho\nabla\cdot(\rho^{-1}\nabla) + \omega^2/c^2$. Here j is the imaginary unit, ω denotes angular frequency and the circumflex denotes the frequency domain. We write $\hat{G} = \hat{G}^d + \hat{G}^s$, where superscripts d and s stand for direct and scattered, respectively. We define the reflection response at the surface in terms of $\hat{G}^s$ via

$$\hat{R}(\mathbf{x}_R, \mathbf{x}_S, \omega)\hat{s}(\omega) = \frac{2}{j\omega\rho_1}\frac{\partial\hat{G}^s(\mathbf{x}_R, \mathbf{x}_S, \omega)}{\partial z_S}\hat{s}(\omega), \quad (1)$$

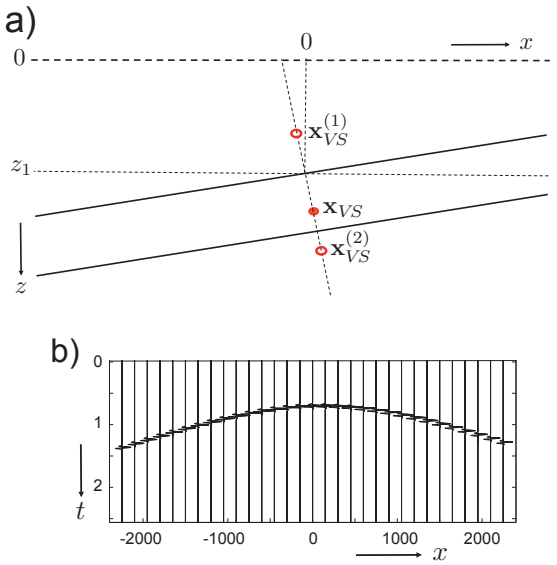

Figure 1. (a) Configuration with two dipping reflectors. (b) Direct arrivals of the response to the virtual source at $\mathbf{x}_{VS}$.

for $z_R = z_S = 0$. Here $\hat{s}(\omega)$ is the spectrum of the source wavelet $s(t)$. Note that (apart from a factor -2) $\hat{R}(\mathbf{x}_R, \mathbf{x}_S, \omega)\hat{s}(\omega)$ represents the pressure at $\mathbf{x}_R$, related to a force source at $\mathbf{x}_S$ or, via reciprocity, the particle velocity at $\mathbf{x}_S$, related to a point source of volume injection rate at $\mathbf{x}_R$. Since we assumed that the acquisition surface is transparent, no surface-related multiples are present in the reflection response. Hence, $\hat{R}(\mathbf{x}_R, \mathbf{x}_S, \omega)\hat{s}(\omega)$, or in the time domain $R(\mathbf{x}_R, \mathbf{x}_S, t) * s(t)$ (the asterisk denotes convolution), can be obtained from the measured reflection data by surface-related multiple elimination (Verschuur et al., 1992).

The aim of the proposed method is to use the deconvolved reflection response $R(\mathbf{x}_R, \mathbf{x}_S, t)$ to retrieve the virtual-source response $G(\mathbf{x}, \mathbf{x}_{VS}, t)$, with $\mathbf{x}_{VS}$ in the subsurface and $\mathbf{x}$ at the surface. As mentioned in the introduction, apart from the reflection response we need an estimate of the direct arrivals. For the constant velocity model of Figure 1a, the high-frequency approximation of the Fourier transform of the direct Green's function $G^d(\mathbf{x}, \mathbf{x}_{VS}, t)$ is given by $\hat{G}^d(\mathbf{x}, \mathbf{x}_{VS}, \omega) = t_1^- \rho_2 \hat{G}_0^d(\mathbf{x}, \mathbf{x}_{VS}, \omega)$, with

$$\hat{G}_0^d(\mathbf{x}, \mathbf{x}_{VS}, \omega) = j\omega\frac{\exp\{-j(\omega|\mathbf{x} - \mathbf{x}_{VS}|/c + \mu\pi/4)\}}{\sqrt{8\pi|\omega||\mathbf{x} - \mathbf{x}_{VS}|/c}}, \quad (2)$$

with $\mu = \text{sign}(\omega)$. Note that the scaled direct Green's function $\hat{G}_0^d(\mathbf{x}, \mathbf{x}_{VS}, \omega)$ requires only information on the propagation velocity c and not on the position and properties of the interfaces. Figure 1b shows $G_0^d(\mathbf{x}, \mathbf{x}_{VS}, t) * s_0(t)$, where $s_0(t)$ is a zero-phase wavelet (here a Ricker wavelet with a central frequency of 20 Hz). In the following procedure the convolution with $s_0(t)$ is optional, but in practice this wavelet will help to compensate for

the fact that the reflection response is deconvolved for the source wavelet $s(t)$. If $s_0(t)$ is included, it is essential that is zero phase.

4 INITIATING THE ITERATIVE PROCESS

The iterative process is started by defining an initial incident downgoing wave field at $z = 0$ as the time-reversed version of the direct arrivals, hence, $p_0^+(\mathbf{x}, t) = A^{(0)} G_0^d(\mathbf{x}, \mathbf{x}_{VS}, -t) * s_0(t)$, with $A^{(0)} = 1$, see Figure 2a for $t < 0$. The reflected upgoing wave field is obtained by convolving the incident field with the deconvolved reflection response and integrating over the source positions, according to

$$p_0^-(\mathbf{x}_R, t) = \int_{-\infty}^{\infty} \left[R(\mathbf{x}_R, \mathbf{x}, t) * p_0^+(\mathbf{x}, t) \right]_{z=0} \mathrm{d}x, \qquad (3)$$

for $z_R = 0$. We analyze this integral with stationary-phase arguments, starting with the response of the first reflector (a more detailed derivation is given in the Appendix. Figure 2b shows a number of rays, leaving different sources at the surface, reflecting at the first reflector, and arriving at one and the same receiver at $\mathbf{x}_R$. According to equation (3), these reflection responses are convolved with the initial incident field, of which the rays are also shown in Figure 2b (these are the rays that converge in $\mathbf{x}_{VS}$). This convolution product is stationary for the source at $x_0^{(1)}$, where the rays of the incident field and of the reflection response have the same direction. Figure 2c shows a number of such stationary rays for different receiver positions. With simple geometrical arguments it follows that these rays cross each other at the mirror image of the virtual source with respect to the first reflector, i.e., at $\mathbf{x}_{VS}^{(1)} = (-100, 600)$. The traveltimes of the convolution product are given by the length of the rays from $\mathbf{x}_{VS}^{(1)}$ to the surface, divided by the velocity. Hence, it is as if the response of the first reflector to the initial incident field originates from a source at $\mathbf{x}_{VS}^{(1)}$ (this is confirmed by the derivation in the Appendix). This response is thus equal to $A^{(1)} G_0^d(\mathbf{x}_R, \mathbf{x}_{VS}^{(1)}, t) * s_0(t)$, see Figure 2a (the first event for $t > 0$). Here $A^{(n)}$ is defined as the product of reflection and transmission coefficients contributing to the nth event of the reflection response $R(\mathbf{x}_R, \mathbf{x}_S, t)$, hence $A^{(1)} = r_1$.

With similar arguments it follows that the response of the second reflector to the initial incident field apparently originates from a mirror image of the virtual source in the second reflector, i.e., at $\mathbf{x}_{VS}^{(2)} = (200, 1800)$. Hence, it is equal to $A^{(2)} G_0^d(\mathbf{x}_R, \mathbf{x}_{VS}^{(2)}, t) * s_0(t)$, with $A^{(2)} = t_1^- r_2 t_1^+$, see Figure 2a (the second event for $t > 0$). The multiple reflected responses to the initial incident field also apparently originate from mirror images of the virtual source, all located along the line $z = z_1 + x/a$, see Figure 1a. For example, the first multiple is equal to $A^{(3)} G_0^d(\mathbf{x}_R, \mathbf{x}_{VS}^{(3)}, t) * s_0(t)$, with $A^{(3)} = -t_1^- r_2^2 r_1 t_1^+$ and $\mathbf{x}_{VS}^{(3)} = (500, 3000)$ (being the mirror image of $\mathbf{x}_{VS}$ in the mirror image of the first reflector with respect to the second reflector). Figure 2a ($t > 0$) shows the total response $p_0^-(\mathbf{x}, t)$ to the initial incident field $p_0^+(\mathbf{x}, t)$. Because it has been derived with the method of stationary phase this response is free of artifacts. Of course in practice equation (3) needs to be evaluated numerically, which will introduce finite aperture artifacts, etc.

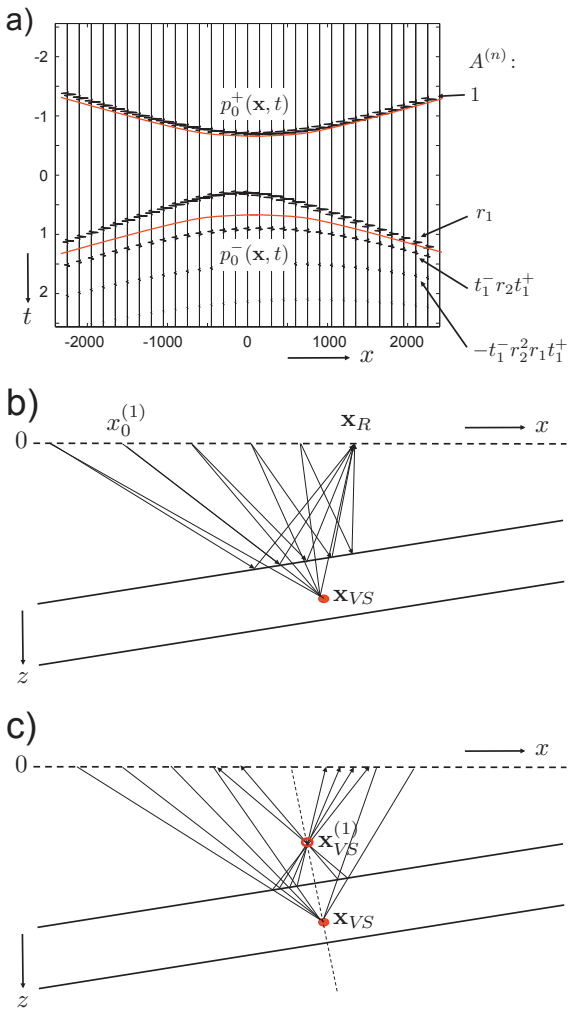

Figure 2. Initiating the iterative process. (a) Initial incident field (the time-reversal of Figure 1b) and its reflection response, both at $z = 0$. (b) Analysis of the response of the first reflector for a fixed receiver at $\mathbf{x}_R$. The stationary point is denoted by $x_0^{(1)}$. (c) Stationary rays (like the one in (b)) for different receivers. The response of the first reflector (indicated by r_1 in (a)) seems to originate from $\mathbf{x}_{VS}^{(1)}$.

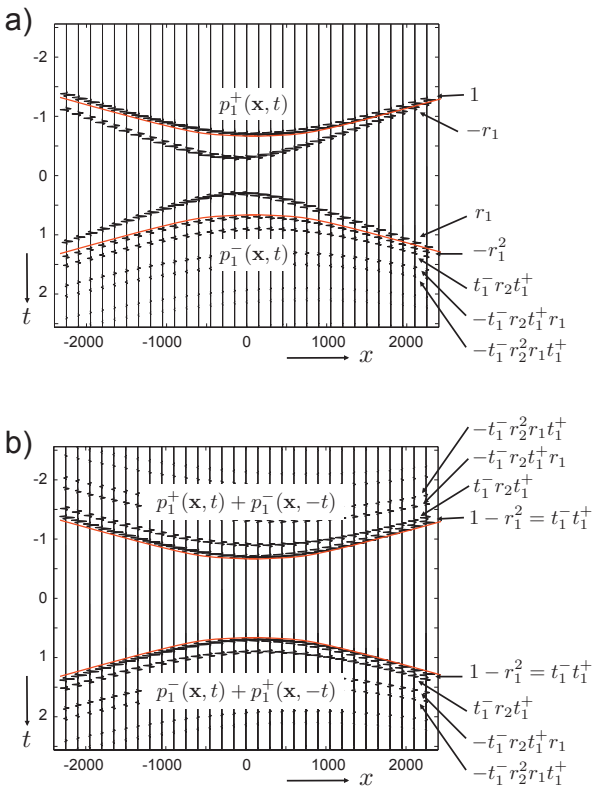

Figure 3. (a) Result of the iterative process. Between the red curves the incident field is minus the time-reversed reflected field. (b) Superposition of total field and its time-reversed version. This field is proportional to $G(\mathbf{x},\mathbf{x}_{VS},t)+G(\mathbf{x},\mathbf{x}_{VS},-t)$.

5 THE ITERATIVE PROCESS

In Figure 2a we define two traveltime curves, indicated by the red solid lines. The upper curve is taken directly after the initial incident field $p_0^+(\mathbf{x},t)$ and the lower curve is defined as the time-reversal of the upper curve (hence, it is taken just before the direct arrival of Figure 1b). We define a window function $w(\mathbf{x},t)$ that equals 1 between these red curves and 0 elsewhere. We discuss an iterative scheme, which has the aim to modify the incident field in such a way that, within the time window, it is equal to minus the time-reversed reflection response. We will motivate this peculiar condition in the next section. To achieve this goal, the kth iteration is defined as follows

$$p_k^+(\mathbf{x},t) = p_0^+(\mathbf{x},t) - w(\mathbf{x},t)p_{k-1}^-(\mathbf{x},-t), \qquad (4)$$

$$p_k^-(\mathbf{x}_R,t) = \int_{-\infty}^{\infty}\left[R(\mathbf{x}_R,\mathbf{x},t) * p_k^+(\mathbf{x},t)\right]_{z=0}\mathrm{d}x, \qquad (5)$$

for $\mathbf{x}$ and $\mathbf{x}_R$ at $z=0$. The reflection response $p_0^-(\mathbf{x},t)$ is shown in Figure 2a ($t>0$). Only the response of the first reflector (indicated by r_1) falls within the time window. Hence, for $k=1$ we have $w(\mathbf{x},t)p_0^-(\mathbf{x},-t) = r_1 G_0^d(\mathbf{x},\mathbf{x}_{VS}^{(1)},-t) * s_0(t)$. Subtracting this from $p_0^+(\mathbf{x},t)$ gives, according to equation (4), the modified incident wave field $p_1^+(\mathbf{x},t)$. This is shown in Figure 3a ($t<0$). Using equation (5) we evaluate the reflection response to this modified incident wave field. This reflection response is the superposition of $p_0^-(\mathbf{x}_R,t)$, evaluated in the previous section, and the response to $-r_1 G_0^d(\mathbf{x},\mathbf{x}_{VS}^{(1)},-t) * s_0(t)$. Following the same reasoning as in the previous section, the first two terms of this additional response seem to originate from mirror images of $\mathbf{x}_{VS}^{(1)}$ in the first and second reflector, hence, from $\mathbf{x}_{VS}^{(1,1)} = \mathbf{x}_{VS}$ (the original virtual source) and $\mathbf{x}_{VS}^{(1,2)} = (400, 2600)$, respectively. The amplitude factors of these two terms are $-A^{(1)}r_1 = -r_1^2$ and $-A^{(2)}r_1 = -t_1^- r_2 t_1^+ r_1$, respectively. Higher order terms are evaluated in a similar way. Figure 3a ($t>0$) shows the reflection response $p_1^-(\mathbf{x},t)$, with the amplitude factors of the different events indicated in the right margin. Note that within the time window (i.e., between the red curves) $p_1^-(\mathbf{x},t)$ is identical to $p_0^-(\mathbf{x},t)$, hence further iterations will not cause any changes. Already after one iteration we have achieved the desired situation mentioned at the beginning of this section. This is a consequence of analyzing the simple configuration of Figure 1a. For more complex configurations more iterations will be required.

6 CREATING THE VIRTUAL-SOURCE RESPONSE

After finalizing the iterative process, we define $p(\mathbf{x},t)$ as the superposition of the final incident and reflected wave fields. Because, for this example, iteration $k=1$ was the final iteration, we have $p(\mathbf{x},t) = p_1^+(\mathbf{x},t) + p_1^-(\mathbf{x},t)$. This total field is shown in Figure 3a (all t). Note that $p(\mathbf{x},t)$ obeys the wave equation in the inhomogeneous medium of Figure 1a; Figure 3a is just the cross-section of this field at $z=0$. Within the time window the field at $z=0$ is antisymmetric in time (this was the design criterion for the iterative scheme). Hence, if we superpose the total field and its time-reversed version, i.e., $p(\mathbf{x},t)+p(\mathbf{x},-t)$, all events within the time window cancel each other, see Figure 3b. Note that because we consider a lossless medium, $p(\mathbf{x},t)+p(\mathbf{x},-t)$ obeys the wave equation. The causal part of this superposition is equal to $p_1^-(\mathbf{x},t)+p_1^+(\mathbf{x},-t)$ (Figure 3b, $t>0$) and the acausal part is equal to $p_1^+(\mathbf{x},t)+p_1^-(\mathbf{x},-t)$ (Figure 3b, $t<0$). Since time-reversal changes the propagation direction, it follows that the causal part is upward propagating at $z=0$ and the acausal part is downward propagating at $z=0$. The first arrival of the causal part of Figure 3b corresponds with the direct arrival of the response to the virtual source at $\mathbf{x}_{VS}$ (Figure 1b). Given this last observation, combined with the fact that the causal part

is upward propagating at $z = 0$ and that the total field obeys the wave equation in the inhomogeneous medium and is symmetric, it is plausible that the total field is proportional to $G(\mathbf{x}, \mathbf{x}_{VS}, t) + G(\mathbf{x}, \mathbf{x}_{VS}, -t)$. This argumentation holds for more general situations, but we will check it here for the response in Figure 3b. From the procedure that led to this response, we find for the causal part (taking into account that $1 - r_1^2 = t_1^- t_1^+$)

$$\begin{aligned} p_1^-(\mathbf{x}, t) + p_1^+(\mathbf{x}, -t) = \\ t_1^- t_1^+ \{ G_0^d(\mathbf{x}, \mathbf{x}_{VS}, t) + r_2 G_0^d(\mathbf{x}, \mathbf{x}_{VS}^{(2)}, t) - \\ r_2 r_1 G_0^d(\mathbf{x}, \mathbf{x}_{VS}^{(1,2)}, t) - r_2^2 r_1 G_0^d(\mathbf{x}, \mathbf{x}_{VS}^{(3)}, t) \cdots \} * s_0(t), \end{aligned} \tag{6}$$

with the virtual source position and its mirror images defined in sections 4 and 5. It is easily seen that for the configuration of Figure 1a, this is equal to $(t_1^+/\rho_2) G(\mathbf{x}, \mathbf{x}_{VS}, t) * s_0(t)$. Hence, for the total field we have indeed

$$p(\mathbf{x}, t) + p(\mathbf{x}, -t) = \frac{t_1^+}{\rho_2} G_h(\mathbf{x}, \mathbf{x}_{VS}, t) * s_0(t), \tag{7}$$

where $G_h(\mathbf{x}, \mathbf{x}_{VS}, t) = G(\mathbf{x}, \mathbf{x}_{VS}, t) + G(\mathbf{x}, \mathbf{x}_{VS}, -t)$. Note that because G obeys the wave equation $LG = -\rho_2 \delta(\mathbf{x} - \mathbf{x}_{VS}) \frac{\partial \delta(t)}{\partial t}$ (section 3), G_h obeys the homogeneous equation $LG_h = 0$. This is in agreement with the fact that $p(\mathbf{x}, t) + p(\mathbf{x}, -t)$ has been constructed without introducing a singularity at $\mathbf{x}_{VS}$. G_h is called the homogeneous Green's function, after Porter (1970) and Oristaglio (1989) (but note that these authors take the difference instead of the sum of the causal and acausal Green's functions because of a different definition of the source in the wave equation).

7 CONCLUDING REMARKS

For the configuration of Figure 1a we have shown that the iterative scheme of equations (4) and (5), combined with the process discussed in section 6, creates the response to a virtual source in an unknown medium from the reflection response at the surface and an estimate of the direct arrivals.

The iterative scheme of equations (4) and (5) is akin to an iterative solution of inverse scattering methods. As shown in equations (2.27), (3.16), and (5.18) of Burridge (1980), the Gel'fand-Levitan equation, the Marchenko equation and the Gopinath-Sondhi equations of inverse scattering in one dimension can be written (in symbolic notation) as

$$K - F + \int_W KR = 0, \tag{8}$$

where R denotes the reflection data, F a known function that may depend on the reflection data, and K the function that one solves for. The integral $\int_W$ denotes integration over a windowed time interval. The integral equation (8) can be solved by iteration by writing it as $K = F - \int_W KR$ and by inserting the left-hand side into the right-hand side (Ge, 1987). This gives the iterative solution

$$K_k = F - \int_W K_{k-1} R. \tag{9}$$

The iterative system of equations (4) and (5) has the same structure as the iterative scheme (9). The connection between iteration, time-reversal and inverse scattering based on the Marchenko equation in 1D has been clarified in great detail by Rose (2001, 2002a,b). Broggini et al. (2011, 2012) show how to use the 1D scheme to create a virtual source in an unknown medium. Our present work aims at generalizing this to 2D and 3D media that are illuminated from above.

The stationary-phase analysis in this paper gives insight in the mechanism of the 2D iterative scheme and confirms the creation of the virtual-source response for a simple configuration. Following the physical arguments in section 6, it is plausible that the proposed methodology will also apply to more complex environments. Of course the proposed method will also have its limitations. The effects of a finite acquisition aperture, triplications, head waves, diving waves, fine-layering, errors in the direct arrivals, etc. need further investigation. A first numerical test by one of us (FB) with a variable-velocity syncline model shows promising results with respect to the handling of triplications. Errors in the estimated direct arrivals will cause defocusing and mispositioning of the virtual source (similar as in standard imaging algorithms), but we expect that these errors will not deteriorate the reconstruction of the internal multiples (which come from the response of the actual medium).

For those configurations for which the proposed methodology applies, the potential applications are fascinating. The method enables the retrieval of the response to a virtual source in an unknown medium, assuming an estimate of the direct arrivals is available. Since no actual receivers are needed inside the medium, virtual sources can be created anywhere. The virtual-source responses contain all internal multiples, hence the method could be used as a basis to image the subsurface without internal multiple ghosts (Wapenaar et al., 2012). Because the created virtual sources are independent of each other, the prediction and removal of internal multiples will not suffer from error propagation, unlike other imaging methods that aim at internal multiple suppression.

REFERENCES

Bakulin, A. & Calvert, R., 2006. The virtual source method: Theory and case study, *Geophysics*, **71**(4), SI139–SI150.

Broggini, F. & Snieder, R., 2012. Connection of scattering principles: a visual and mathematical tour, *European Journal of Physics*, **33**, 593-613.

Broggini, F., Snieder, R., & Wapenaar, K., 2011. Connection of scattering principles: focusing the wavefield without source or receiver, in *SEG, Expanded Abstracts*, pp. 3845–3850.

Broggini, F., Snieder, R., & Wapenaar, K., 2012. Focusing the wavefield inside an unknown 1D medium - Beyond seismic interferometry, submitted to *Geophysics*.

Burridge, R., 1980. The Gelfand-Levitan, the Marchenko, and the Gopinath-Sondhi integral equations of inverse scattering theory, regarded in the context of inverse impulse-response problems, *Wave Motion*, **2**, 305–323.

de Hoop, A. T., 1995. *Handbook of radiation and scattering of waves*, Academic Press, London.

Ge, D. B., 1987. An iterative technique in one-dimensional profile inversion, *Inverse Problems*, **3**, 399–406.

Oristaglio, M. L., 1989. An inverse scattering formula that uses all the data, *Inverse Problems*, **5**, 1097–1105.

Porter, R. P., 1970. Diffraction-limited, scalar image formation with holograms of arbitrary shape, *Journal of the Optical Society of America*, **60**, 1051–1059.

Rose, J. H., 2001. "Single-sided" focusing of the time-dependent Schrödinger equation, *Physical Review A*, **65**, 012707.

Rose, J. H., 2002a. Time reversal, focusing and exact inverse scattering, in *Imaging of complex media with acoustic and seismic waves*, pp. 97–106, eds Fink, M., Kuperman, W. A., Montagner, J. P., & Tourin, A., Springer, Berlin.

Rose, J. H., 2002b. 'Single-sided' autofocusing of sound in layered materials, *Inverse Problems*, **18**, 1923–1934.

Schuster, G. T., Yu, J., Sheng, J., & Rickett, J., 2004. Interferometric/daylight seismic imaging, *Geophysical Journal International*, **157**, 838–852.

Snieder, R., Wapenaar, K., & Larner, K., 2006. Spurious multiples in seismic interferometry of primaries, *Geophysics*, **71**(4), SI111–SI124.

Verschuur, D. J., Berkhout, A. J., & Wapenaar, C. P. A., 1992. Adaptive surface-related multiple elimination, *Geophysics*, **57**(9), 1166–1177.

Wapenaar, K., Broggini, F., & Snieder, R., 2011. A proposal for model-independent 3D wave field reconstruction from reflection data, in *SEG, Expanded Abstracts*, pp. 3788–3792.

Wapenaar, K., Thorbecke, J., van der Neut, J., Broggini, F., & Snieder, R., 2012. Creating virtual sources inside an unknown medium from reflection data: a new approach to internal multiple elimination, in *EAGE, Extended Abstracts*.

APPENDIX: DETAILS OF THE STATIONARY-PHASE ANALYSIS

We evaluate equation (3) with the method of stationary phase. In the frequency domain this equation reads

$$\hat{p}_0^-(\mathbf{x}_R,\omega) = \int_{-\infty}^{\infty} \big[\hat{R}(\mathbf{x}_R,\mathbf{x},\omega)\hat{p}_0^+(\mathbf{x},\omega)\big]_{z=0}\mathrm{d}x, \quad (A.1)$$

where the incident field $\hat{p}_0^+(\mathbf{x},\omega)$ follows from complex conjugating the right-hand side of equation (2), according to

$$\hat{p}_0^+(\mathbf{x},\omega) = -j\omega\frac{\exp\{j(\omega|\mathbf{x}-\mathbf{x}_{VS}|/c+\mu\pi/4)\}}{\sqrt{8\pi|\omega||\mathbf{x}-\mathbf{x}_{VS}|/c}}\hat{s}_0(\omega), \quad (A.2)$$

with $\mu = \mathrm{sign}(\omega)$. For the reflection response we write $\hat{R}(\mathbf{x}_R,\mathbf{x},\omega) = \sum_{n=1}^{\infty}\hat{R}^{(n)}(\mathbf{x}_R,\mathbf{x},\omega)$, where $\hat{R}^{(n)}$ represents the nth event of the reflection response. Using equation (1) we obtain

$$\hat{R}^{(n)}(\mathbf{x}_R,\mathbf{x},\omega) = \frac{A^{(n)}z_R^{(n)}}{|\mathbf{x}-\mathbf{x}_R^{(n)}|}\frac{j\omega}{c}\frac{\exp\{-j(\omega|\mathbf{x}-\mathbf{x}_R^{(n)}|/c+\mu\pi/4)\}}{\sqrt{2\pi|\omega||\mathbf{x}-\mathbf{x}_R^{(n)}|/c}}. \quad (A.3)$$

For $\hat{R}^{(1)}$, i.e. the primary response of the first reflector, $A^{(1)} = r_1$ and $\mathbf{x}_R^{(1)}$ is the mirror image of $\mathbf{x}_R$ with respect to the first reflector, see Figure A1. For $\hat{R}^{(2)}$, the primary response of the second reflector, $A^{(2)} = t_1^- r_2 t_1^+$ and $\mathbf{x}_R^{(2)}$ is the mirror image of $\mathbf{x}_R$ in the second reflector. For $\hat{R}^{(3)}$, the first multiple, $A^{(3)} = -t_1^- r_2^2 r_1 t_1^+$ and $\mathbf{x}_R^{(3)}$ is the mirror image of $\mathbf{x}_R$ in the mirror image of the first reflector with respect to the second reflector, etc. Equation (A.1) can be written as $\hat{p}_0^-(\mathbf{x}_R,\omega) = \sum_{n=1}^{\infty}\mathcal{I}^{(n)}$, with

$$\mathcal{I}^{(n)} = \int_{-\infty}^{\infty} f(x)\exp\{jk\phi(x)\}\mathrm{d}x, \quad (A.4)$$

where $k = \omega/c$,

$$f(x) = \frac{|\omega|A^{(n)}z_R^{(n)}\hat{s}_0(\omega)}{4\pi l_{VS}^{1/2}\{l_R^{(n)}\}^{3/2}}, \quad \phi(x) = l_{VS} - l_R^{(n)}, \quad (A.5)$$

with

$$l_{VS}(x) = |\mathbf{x}-\mathbf{x}_{VS}| = \sqrt{(x-x_{VS})^2+z_{VS}^2}, \quad (A.6)$$

$$l_R^{(n)}(x) = |\mathbf{x}-\mathbf{x}_R^{(n)}| = \sqrt{(x-x_R^{(n)})^2+(z_R^{(n)})^2}. \quad (A.7)$$

The derivatives of the phase are

$$\phi'(x) = \frac{x-x_{VS}}{l_{VS}} - \frac{x-x_R^{(n)}}{l_R^{(n)}}, \quad (A.8)$$

$$\phi''(x) = \frac{z_{VS}^2}{l_{VS}^3} - \frac{(z_R^{(n)})^2}{\{l_R^{(n)}\}^3}. \quad (A.9)$$

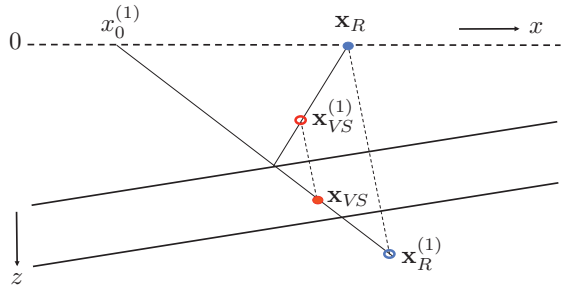

Figure 4. Configuration for the stationary-phase analysis of equation (10) for $n = 1$.

The point $x_0^{(1)}$ depicted in Figure A1 obeys

$$\frac{x_0^{(1)} - x_{VS}}{z_{VS}} = \frac{x_0^{(1)} - x_R^{(1)}}{z_R^{(1)}}. \tag{A.10}$$

Generalized for $x_0^{(n)}$, this gives

$$x_0^{(n)} = \frac{x_{VS} z_R^{(n)} - x_R^{(n)} z_{VS}}{z_R^{(n)} - z_{VS}}. \tag{A.11}$$

Substitution into equation (A.8) gives $\phi'(x_0^{(n)}) = 0$, hence, $x_0^{(n)}$ is the stationary point of $\phi(x)$. According to equations (A.6) and (A.7) we have

$$l_{VS}(x_0^{(n)}) = \frac{z_{VS}}{z_R^{(n)} - z_{VS}} |\mathbf{x}_R^{(n)} - \mathbf{x}_{VS}|, \tag{A.12}$$

$$l_R^{(n)}(x_0^{(n)}) = \frac{z_R^{(n)}}{z_R^{(n)} - z_{VS}} |\mathbf{x}_R^{(n)} - \mathbf{x}_{VS}|. \tag{A.13}$$

In the main text we define $\mathbf{x}_{VS}^{(n)}$ as a mirror image of $\mathbf{x}_{VS}$, obtained in the same way as $\mathbf{x}_R^{(n)}$ is obtained by mirroring $\mathbf{x}_R$. This implies that $|\mathbf{x}_R^{(n)} - \mathbf{x}_{VS}| = |\mathbf{x}_R - \mathbf{x}_{VS}^{(n)}|$. This is illustrated for $n = 1$ in Figure A1. Hence, the stationary-phase approximation of equation (A.4) is (for large $|k|$)

$$\begin{aligned} \mathcal{I}^{(n)} &\approx \sqrt{\frac{2\pi}{|k\phi''(x_0^{(n)})|}} f(x_0^{(n)}) \exp\{j(k\phi(x_0^{(n)}) + \mu\pi/4)\} \\ &= j\omega A^{(n)} \frac{\exp\{-j(\omega|\mathbf{x}_R - \mathbf{x}_{VS}^{(n)}|/c + \mu\pi/4)\}}{\sqrt{8\pi|\omega||\mathbf{x}_R - \mathbf{x}_{VS}^{(n)}|/c}} \hat{s}_0(\omega). \end{aligned} \tag{A.14}$$

Hence,

$$\hat{p}_0^-(\mathbf{x}_R, \omega) = \sum_{n=1}^{\infty} \mathcal{I}^{(n)} = \sum_{n=1}^{\infty} A^{(n)} \hat{G}_0^d(\mathbf{x}_R, \mathbf{x}_{VS}^{(n)}, \omega) \hat{s}_0(\omega), \tag{A.15}$$

with $\hat{G}_0^d(\mathbf{x}_R, \mathbf{x}_{VS}^{(n)}, \omega)$ as defined in equation (2), but with the source at $\mathbf{x}_{VS}^{(n)}$.